Journal of Innovative Technology, Vol. 3, No. 2, pp. 1-5, September 2021
http://doi.org/10.29424/JIT.202109_3(2).0001

Analysis and Design of a Zero-Voltage-Switching PWM DC-DC Converter without Auxiliary Circuit

Chien-Ming Wang [1*], Chih-Yen Lin [2], and Hung-Lin Wang [3]

ABSTRACT

This paper proposes a family of zero-voltage-switching (ZVS) pulse-width-modulated (PWM) dc-dc converters with no auxiliary circuit. The proposed converters do not require any auxiliary ZVS circuit to provide ZVS functions to the switches. This development reduces costs in production and the system maintains a power efficiency of greater than 96% at rated load. The proposed converter operates at a constant frequency, and all switches have on and off ZVS. In comparison to the hard switching converter counterpart, this system has no overvoltage across the switches and no additional current stress. The theory of the ZVS-PWM was proposed and a prototype was constructed and tested. Testing and analysis of the prototype confirmed the actual ability of this family of ZVS-PWM converters.

Keywords: Pulse-width-modulated (PWM), dc-dc converters.

1. INTRODUCTION

Pulse width modulated (PWM) dc-dc converters that are commonly found in industrial settings require higher power density and faster transient response. To achieve this aim, they must increase switching frequency, but this switching results in switching losses and electromagnetic interference (EMI). To mitigate these problems, soft-switching techniques such as zero-voltage-switching (ZVS) and zero-current-switching (ZCS) have been proposed and tested (Elasser and Torrey 1996; Hua *et al.* 1994; Jain *et al.* 2004; Stein and Hey 2000; Tseng and Chen 1998). Frequently these systems add a resonant auxiliary circuit to a conventional PWM converter to achieve the soft-switching function. Because the processing time is very short, they are able to retain their original operational characteristics. Some of the auxiliary circuits however, still generate substantial switching losses and EMI noise as their switches operate under hard-switching conditions. Although some designs have improved this shortcoming, there are still additional voltage and/or current stresses on the main power semiconductors in the converters.

This paper proposes a novel ZVS PWM approach with several key improvements over the existing designs. Although the proposed ZVS PWM method does not use an auxiliary circuit, all thee switches in the converter operate under ZVS condition. A family of dc-dc ZVS PWM converters based on ZVS PWM are proposed and diagrams are presented in Fig. 1. These circuits operate at a constant frequency. Moreover, the switches in them have no additional voltage and current stress, making them more efficient than existing hard-switching converters. Taking the ZVS PWM boost dc-dc boost converter as an example, this paper undertakes an analysis of the design and presents the design guidelines. The experimental results in this paper verify the performance of the family of the tested ZVS-PWM converters.

2. THE PROPOSED ZVS-PWM METHOD AND CIRCUIT OPERATION PRICIPLE

The family of dc-dc ZVS PWM converters based on the method shown are presented in Fig. 1. The proposed ZVS PWM method replaces the diode in the conventional PWM dc-dc converter with a MOSFET switch M_B, to make the switch current bidirectional. Moreover, because the dc-dc ZVS PWM converters operate at a constant frequency and in a continuous conduction mode (CCM), the inductor currents iL are bipolar when generating ZVS resonance. It should be noted that the principle operational features of this dc-dc ZVS PWM converter family, are the same as for the ZVS PWM boost converter. The ZVS PWM boost converter shown in Fig. 1(b) is used as example for this paper.

2.1 Stage of Operation of the ZVS-PWM Boost Converter

For simplification of analysis, it is assumed that the converter operates in a steady-state. Furthermore, the value of C is large enough to be assumed and V_o is constant and ripple free. Before $t = t_0$, $v_{CrA}(t)$ and $v_{CrB}(t)$ are equal to V_o and zero, respectively. Based on these assumptions, circuit operations in one switching cycle can be divided into six stages. The six dynamic equivalent circuits of the ZVS PWM boost converter during one switching period are shown in Fig. 2, where MA starts conducting at $t = t_1$, and then turns off at $t = t_3$. MB starts conducting at $t = t_4$, and then turns off at $t = t_6$. The ideal resultant waveforms of the ZVS PWM boost are shown in Fig. 3. Before $t = t_0$, the switch MA is off, and the switch M_B is on, the current i_L flows through M_B and V_o.

Manuscript received May 10, 2021; accepted May 10, 2021.

[1*] Professor (corresponding author), Department of Electrical Engineering, National I-Lan University, Taiwan 26047, R.O.C. (e-mail: cmwang @niu.edu.tw).

[2] Student, Department of Electrical Engineering, National I-Lan University, Taiwan 26047, R.O.C.

[3] Student, Department of Electronic Engineering, Chung Yuan Christian University, Taiwan 32023, R.O.C.

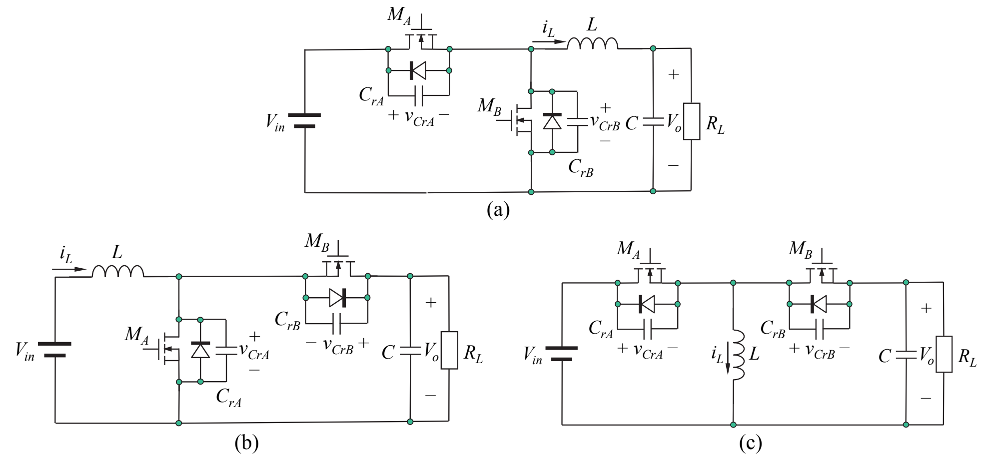

Fig.1 Topologies of three basic ZVS-PWM converter, (a) buck converter, (b) boost converter, and (c) buck-boost converter.

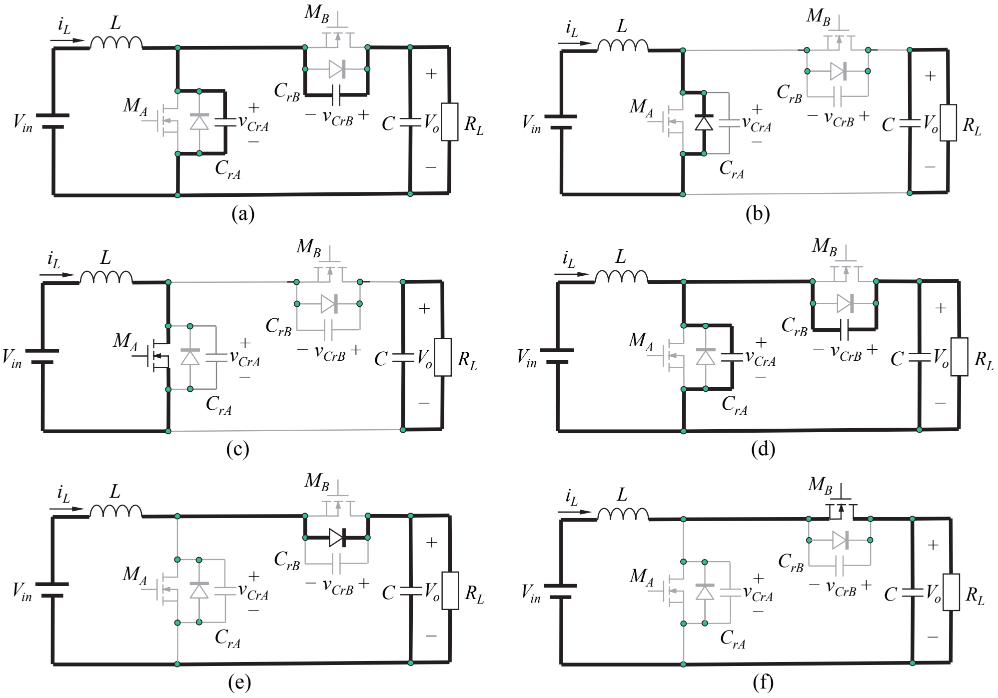

Fig. 2 Topology stages of the demonstrated ZVS-PWM boost converter

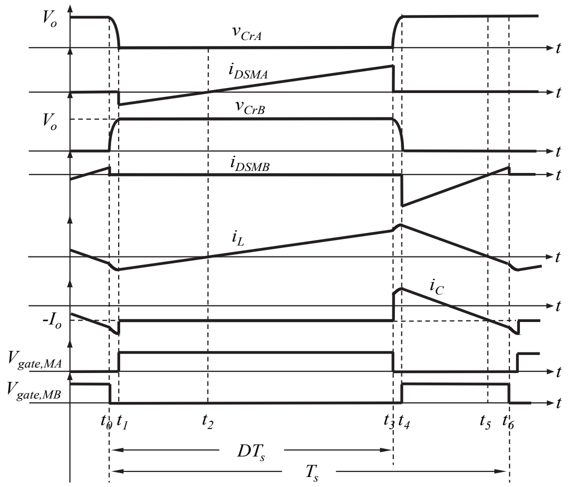

Fig. 3 Ideal waveforms of the ZVS-PWM boost converter.

STAGE 1 [Fig. 2(a): $t_0 < t < t_1$]: This stage begins as M_B turns off, and ZVS is at $t = t_0$. L, C_{rA} and C_{rB} start resonant operation. i_L decreases from $i_L(t_0)$. v_{CrA} decreases from V_o and v_{CrB} increases from zero. The stage ends as $vC_{rA}(t)$ drops to zero and $v_{CrB}(t)$ reaches V_o at $t = t_1$. Moreover, the body diode of M_A turns on with ZVS. The M_A activates and turns on with ZVS.

$$i_L(t) = \frac{V_{in}}{Z_o} \sin\omega\,(t - t_0) + i_L(t_0)\cos\omega\,(t - t_0) \tag{1}$$

$$v_{CrA}(t) = V_{in}\,(1 - \cos\omega\,(t - t_0)) + Z_o i_L\,(t_0)\sin\omega\,(t - t_0) \tag{2}$$

$$v_{CrB}(t) = V_o - v_{CrA}(t)$$

$$\text{where } \omega\,(t - t_0) = 1/\sqrt{L\,(C_{rA} + C_{rB})} \tag{3}$$

$$\text{and } Z_o = \sqrt{L\,(C_{rA} + C_{rB})}$$

STAGE 2 [Fig. 2(b): $t_1 < t < t_2$]: During this stage, the circuit operation is the same as the on state of a conventional converter. L charges linearly by V_{in}. $i_L(t)$. $i_L(t1)$ increases linearly via V_{in}, L and the body diode M_A. $v_{CrA}(t)$ and $v_{CrB}(t)$ remain at zero, and V_o, respectively. This stage ends when $i_L(t)$ reaches zero.

$$i_L(t) = i_L(t_0) + \frac{V_{in}}{L}(t - t_1) \tag{4}$$

$$v_{CrA}(t) = 0 \tag{5}$$

$$v_{CrB}(t) = V_0 \tag{6}$$

STAGE 3 [Fig. 2(c): $t2 < t < t3$]: This stage begins when the polarity of the inductor current changes from negative to positive. The charging path of L is changes from V_{in}, L and the body diode M_A, to V_{in}, L and M_A. This stage keeps the circuit operation in Stage 2. Thus, i_L(t) undergoes a continuous and linear increase. $v_{CrA}(t)$ and v_{CrB}(t) remain at zero and V_o, respectively. This stage ends when the proposed converter completes the duty cycle.

$$i_L(t) = i_L(t_0) + \frac{V_{in}}{L}(t - t_1) \tag{7}$$

$$v_{CrA}(t) = 0 \tag{8}$$

$$v_{CrB}(t) = V_0 \tag{9}$$

STAGE 4 [Fig. 2(d): $t_3 < t < t_4$]: This stage begins when M_A turns off by ZVS at $t = t_3$. L, C_{rA} and C_{rB} begin resonant operation again. i_L increases from $i_L(t_3)$. v_{CrA} increases from zero, and v_{CrB} decreases from V_o. This stage ends when $v_{CrB}(t)$ drops to zero and $v_{CrA}(t)$ reaches V_o at $t = t_4$. The body diode of M_B activates by ZVS. M_B can also be triggered to turn-on state by ZVS.

$$i_L(t) = \frac{V_{in} - V_o}{Z_o}\sin\omega(t - t_3) + i_L(t_3)\cos\omega(t - t_3) \tag{10}$$

$$\begin{aligned} v_{CrA}(t) = {} & (V_{in} - V_o)(1 - \cos\omega(t - t_3)) \\ & + Z_o i_L(t_3)\sin\omega(t - t_3) \end{aligned} \tag{11}$$

$$v_{CrB}(t) = V_o - v_{CrA}(t) \tag{12}$$

STAGE 5 [Fig. 2(e): $t_4 < t < t_5$]: During this stage, the circuit operation of the proposed converter is the same as in the inactive state of the conventional converter. L is discharged linearly across $V_{in}–V_o$. $i_L(t)$ decreases linearly from $i_L(t_4)$ via V_{in}, L, the body diode M_B and V_o. $v_{CrA}(t)$ and $v_{CrB}(t)$ remain at V_o and zero, respectively. This stage ends when $i_L(t)$ drops to zero.

$$i_L(t) = i_L(t_4) + \frac{V_{in} - V_o}{L}(t - t_4) \tag{13}$$

$$v_{CrA}(t) = V_0 \tag{14}$$

$$v_{CrB}(t) = 0 \tag{15}$$

STAGE 6 [Fig. 2(f): $t_5 < t < t_6$]: This stage begins when the polarity of the inductor current changes from positive to negative. The discharge path of L changes from V_{in}, L, the body diode of M_B and V_o, to V_{in}, L, M_B and V_o. This keeps the circuit in stage 5. $i_L(t)$ continues to decrease linearly. $v_{CrA}(t)$ and $v_{CrB}(t)$ remain at V_o and zero, respectively. This stage ends when the next period begins.

$$i_L(t) = i_L(t_4) + \frac{V_{in} - V_o}{L}(t - t_4) \tag{16}$$

$$v_{CrA}(t) = V_0 \tag{17}$$

$$v_{CrB}(t) = 0 \tag{18}$$

At $t = t_6$, the circuit operation returns to Stage 1.

2.2 Output Characteristics

The integral of the input inductor voltage in one switching period is zero under steady-state operation. This is governed by the Equation (19).

$$\int_0^{T_s} v_L\,dt = 0 \tag{19}$$

Thus, the voltage conversion ratio $M = Vo/V_{in}$ is obtained by the following:

$$M = \frac{1 - (\Delta t_1 + \Delta t_4)/T_s}{1 - D - (\Delta t_1 + \Delta t_4)/2T_s} \tag{20}$$

where

$$\Delta t_1 \equiv t_1 - t_0 = \frac{1}{\omega}\left\{\cos^{-1}\frac{1}{\sqrt{1 + \left(\frac{z_o i_L(t_0)}{V_{in}}\right)^2}}\right. \\ \left. tan^{-1}\frac{z_o i_L(t_3)}{V_o - V_{in}}\right\} \tag{21}$$

$$\Delta t_4 \equiv t_4 - t_3 = \frac{1}{\omega}\left\{\cos^{-1}\frac{(10)_{ZV_o - V_{in}}}{\sqrt{(V_{in} - V_o)^2 + z_o i_L(t_3)^2}} + \right. \\ \left. tan^{-1}\frac{-z_o i_L(t_3)}{V_o - V_{in}}\right\} \tag{22}$$

where D is the duty cycle of control, $T_s = 1/f_s$ is the switching period, and fs is the switching frequency. The time intervals Δt_1 and Δt_4 derived from (21) and (22) are very small. Thus the voltage conversion ratio $M = V_o/V_{in}$ of the proposed converter is close to that of a conventional dc-dc boost converter.

2.3 Commutation Analysis

The following inequalities must be satisfied in order for the switches to acquire their ZVS properties.

$$L < \frac{V_{in}}{2I_{in,\max}} DT_s \tag{23}$$

where $I_{in,\max}$ is input maximum average current.

3. REALIZATION AND EXPERIMENTAL RESULTS

A prototype 500W ZVS-PWM boost converter was designed and produced. Its design procedure is described in the following steps.

Step 1 — Input and output data specification.

- The input voltage $V_{in} = 100\text{VDC}$;
- The output voltage $V_o = 400\text{VDC}$;
- The maximum output power $P_{o,\max} = 500\text{W}$.
- The switching frequency $f_s = 100$ kHz

Step 2 — Calculation of the maximum input current.

The input maximum current $I_{in,\max}$ is given by $I_{in,\max} = P_{o,\max}/V_{in} = 5\text{A}$.

Step 3 — Calculation of the resonance parameters.

The inequalities in (23) need to be satisfied to achieving the ZVS function. Thus:

$$L < \frac{V_{in}}{2I_{in,\max}} DT_s = 75\mu\text{H} \tag{24}$$

where $L = 50\mu\text{H}$ was selected for this example.

The resonant frequency $f_r = 5f_s$ was chosen to minimize the influence of the resonance parameters. Thus:

$$\omega = \frac{1}{\sqrt{L(C_{rA} + C_{rB})}} = 3141592.654\text{rad}/\text{s} \tag{25}$$

and

$$C_{rA} = C_{rB} = 1.103nF. \tag{26}$$

such that $C_{rA} = C_{rB} = 1nF$ was selected for the example.

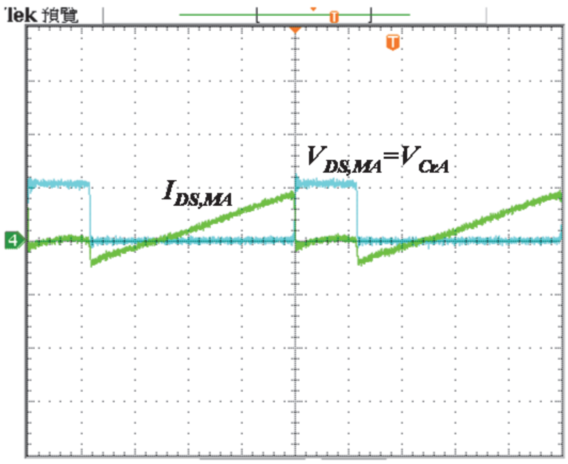

(a)

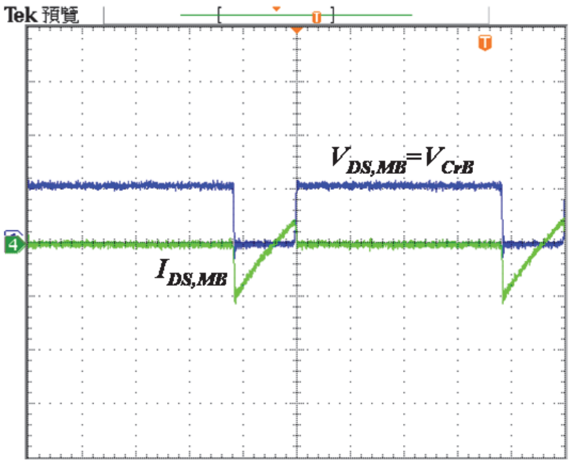

(b)

Fig. 4 **Waveforms of the voltage across the switch and the current through the switch. (V_{MA}, V_{MB}: 400V/div; I_{MA}, I_{MB}: 10A/div, time: 2μs) (a) Switch M_A. (b) Switch M_B**

Step 4 — Selection of the output capacitor was determined by attempting to minimize output ripple. Capacitance C at the output was specified as $C = 470\mu F$.

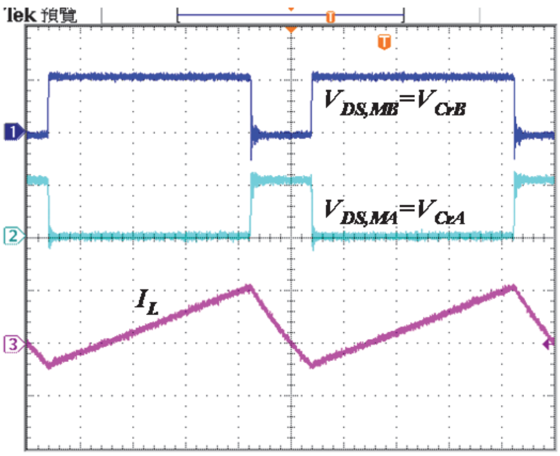

Fig. 5 **Waveforms of resonant capacitor voltage and resonant inductor current.**

MOSFET IRFP 460A power switches were used in this prototype. The voltage waveforms vDS across the switches, and the current iDS through the switches were measured and are presented in Fig. 4. The commutation phenomenon in the switches (MA and MB) demonstrates that the ZVS function was successfully achieved at a constant frequency, and this is also shown in Fig. 4. The switching losses for the main switches in this prototype ZVS-PWM boost converter are practically zero. The waveform of the resonant inductor current and resonant capacitor voltage are shown in Fig. 5. The efficiency of the proposed ZVS-PWM boost converter was measured at approximately 96.3% of rated load.

4. CONCLUSION

Three basic ZVS-PWM converters with a simple and compact configuration were proposed in this paper. The ZVS-PWM boost converter is one such example. Its circuit operation was analyzed. All semiconductor devices in the proposed ZVS-PWM converter switches operated under ZVS conditions. Conventional PWM techniques were used in the proposed converter; therefore, the proposed ZVS-PWM converter does not need any auxiliary ZVS circuit, and retains the features of a ZVS-PWM device. The high power efficiency, which exceeded 96% at rated power load, was confirmed empirically. The prototype successfully demonstrated the initial theories proposed in Section 1.

REFERENCES

Elasser A. and Torrey D.A., (1996). “Soft switching active snubbers for dc/dc converters,” *IEEE Trans. Power Electron*, **11**(5), 710-722.

Hua G., Leu C.S., Jiang Y., and Lee F.C., (1994). “Novel zero-voltage-transition PWM converter,” *IEEE Trans. Power Electron*, **9**(2), 213-219.

Jain N., Jain P.K., and Joos G., (2004). “A Zero Voltage Transition Boost Converter Employing a Soft Switching Auxiliary Circuit with Reduced Conduction Losses,” *IEEE Trans. Power Electron*, **19**(1), 130-139.

Stein C.M. de O. and Hey H.L., (2000) “A True ZCZVT Commutation Cell for PWM Converter,” *IEEE Trans. Power Electron*, **15**(1), 185-193.

Tseng C.J. and Chen C.L., (1998) “Novel ZVT-PWM Converter with Active Snubbers,” *IEEE Trans. Power Electron*, **13**(5), 861-869.